Journal of Porous Media, 25(10):67–81 (2022)

NONSIMILAR FORCED CONVECTION ANALYSIS OF CHEMICALLY REACTIVE MAGNETIZED EYRING-POWELL NANOFLUID FLOW IN A POROUS MEDIUM OVER A STRETCHED RIGA SURFACE

Jifeng Cui,[1,*] Raheela Razzaq,[2] Fakhra Azam,[2] Umer Farooq,[2] Muzamil Hussain,[2,3] & Ali J. Chamkha[4]

[1]*College of Science, Inner Mongolia University of Technology, Hohhot 010051, China*
[2]*Department of Mathematics, COMSATS University Islamabad, Park Road, Chak Shahzad, Islamabad 44000, Pakistan*
[3]*Department of Mathematics, University of the Poonch Rawalakot, Rawalakot 123350, Pakistan*
[4]*Faculty of Engineering, Kuwait College of Science and Technology, Doha District, Kuwait*

*Address all correspondence to: Jifeng Cui, College of Science, Inner Mongolia University of Technology, Hohhot 010051, China, E-mail: cjf@imut.edu.cn

Original Manuscript Submitted: 10/27/2021; Final Draft Received: 2/25/2022

Flows across porous medium have vital roles due to their implementations in the fields of biology and environmental systems. The objective of the current article is to investigate the forced convection of magnetized Eyring-Powell nanofluid flow in a porous medium above a Riga surface through nonsimilar modeling. The current model assumes viscous dissipation, activation energy, chemical reaction, heat generation, and convective boundary conditions. The Riga plate is presented as an electromagnetic actuator based on permanent magnets and recurring conducts of electrodes placed on the plane of the sheet. In nonsimilar flows, the basic quantities vary in the flow direction. The system describing Eyring-Powell models are transmuted into dimensionless nonsimilar form by the utilization of nonsimilar transformations. The nonsimilar system is analytically simulated by employing local nonsimilarity (LNS) up to the second order of iteration and numerically via bvp4c. It is explored that the temperature field represents an escalating manner for distinct variations of Eckert number and radiation parameter. The modified Hartman number and Eckert number enhances both velocity and temperature. The Eckert number expands the concentration portrayal of nanoparticles. Furthermore, the thermophoresis and Brownian factors of nanofluid with activation energy are investigated. The shear stress of the wall expands for the values of the Eyring-Powell parameter and modified Hartmann number. The values of flow, heat, and mass transfer rate for distinct parameters are also illustrated in tables. In limited cases, excellent agreement is found between the present work and published articles.

KEY WORDS: *Eyring-Powell fluid, activation energy, Riga plate, nonsimilar modeling, porous medium*

1. INTRODUCTION

The current study assures that nanofluids attain much attention in industrial and technological fields. Nanofluids contain base fluid with tiny nanosized particles called nanoparticles. Nanofluids are found in thin liquid suspensions of nanoparticles in ordinary fluid. It is investigated that nanofluids have increased thermophysical properties, for instance, viscosity, convective heat transfer coefficients, thermal conductivity, and thermal diffusivity, in contrast to base fluids such as oil or water, etc. (Yu et al., 2008; Tyler et al., 2016; Das et al., 2006). Due to high thermal conductivity, nanofluids have been investigated as working fluids instead of base fluids. Nanofluids have a great number of

1091–028X/22/$35.00

NOMENCLATURE

T_∞	temperature distribution [K]	C_p	heat capacity of fluid [K^{-1} s^{-2} m^2]
f, θ, ϕ	dependent variables		
Gr	Grashof number		
D	mass diffusion coefficient	**Greek Symbols**	
Re_x	local Reynolds number	α	thermal diffusivity [m^2 s^{-1}]
D_B	Brownian diffusion coefficient	ν	kinematic viscosity [m^2 s^{-1}]
M_o	magnetization in magnet	ξ	nonsimilarity variable
σ	electrical conductivity of the fluid	τ	heat capacity
C_∞	concentration distribution	Ψ	stream function
C_f	skin friction coefficient	q_r	radiative heat flux
N_b	Prandtl number	Nu_x	local Nusselt number
Pr	Schmidt number	Nt	thermophoresis parameter
Sc	uniform magnetic field	Sh	local Sherwood number
L	reference length [m]	I	condition at the wall
J_o	density of applied current		
Ec	Eckert number	**Subscripts**	
U_o	reference velocity	∞	ambient condition
u, v	velocity component in the x and y directions [m s^{-1}]	**Superscript**	
B_o	Brownian motion parameter	$'$	differentiation with respect to η

automotive applications, such as in engine oils, coolants, lubricants, etc. Choi (1995) and Das et al. (2003) exposed the most remarkable characteristic of nanofluids, that their thermal conductivity is dependent on temperature. Nanofluids are extensively used in energy and biomedical applications (nano-drug delivery, cancer therapeutics, nano cryosurgery). Shawgo et al. (2002) and Tiwari and Das (2007) introduced a nanofluid model to examine the rate of heat transfer and nanofluid flow with a mixture of nanoparticles. Buongiorno (2006) examined the effect of convective transport in nanofluid by observing the heat transmission properties of the thermophoresis and Brownian motion. Numerous studies are presented in the literature to demonstrate the uses of nanofluids in various fields (Sheikholeslami et al., 2014; Turkyilmazoglu, 2002; Ghalambaz et al., 2019, 2020; Ali, 2021; Abid et al., 2021).

The effects of magnetic fields play a vital role in fluid mechanics because of their numerous applications in the magnification of the thermophysical features of fluid. Numerous fluids that are poor conductors of electricity have been encountered in earth sciences and astronomy. Hence, an extrinsic factor is always required to induce the heat transmission phenomenon across finer conductivity and other connected thermophysical characteristics. A magnetic bar or a continuously stable array of similar magnets with alternating electrodes could be used as the outside force, as illustrated by Khan et al. (2021). Waqas et al. (2020) explained the conduct of magnetic dipole and activation energy along with a flexible sheet to explain the relevance of fluid receiving the development of a magnetic field. Hayat et al. (2016) researched the flow of nanofluid over the Riga plate.

Several fluids having non-Newtonian traits, particularly in the chemical processing industry, include oils, paints, shampoos, soaps, etc. Researchers face difficulties in interpreting non-Newtonian fluids. Numerous fluids are nonlinear in nature. The fundamental relations for such fluids result in complex equations. To deal with such complications, different non-Newtonian fluids models have been devised. The Eyring-Powell fluid model (Ray et al., 2020; Powell and Eyring, 1944) is one example of a complex non-Newtonian fluid model. In comparison to other models, the assumed Eyring-Powell fluids model is well defined. Powell-Eyring fluid heat transmission are prime players in geophysical processes, environmental pollution, and thermal insulation. The model presenting Eyring-Powell fluid flow over an expanding sheet is explored by Javed et al. (2013). Eldabe et al. (2003) explored the impacts of coupled

stresses in the unidirectional flow of Eyring-Powell liquid via moving parallel plates. Mushtaq et al. (2013) assumed an Eyring-Powell fluid flow and analyzed the influences of an exponentially expanding sheet. They looked at the effects of viscoelastic characteristics on thermal and velocity boundary layers in the opposite direction. Rahimi et al. (2017) used the collocation approach to approximate the boundary layer of the Powell-Eyring fluid. Akbar et al. (2015) provided the numerical solutions of the Powell-Eyring magnetofluid above an expanding sheet. The effects of MHD and Newtonian heating on Powell-Eyring fluid over a stretched cylinder were demonstrated by Hayat et al. (2018). Ghadikolaei et al. (2017) showed the time-dependent behavior of a magnetized flow of Eyring-Powell fluid squeezed by a channel under the factor of Joule dissipation. Gholinia et al. (2013) explained the magnetic flow of the Eyring-Powell fluid, which is formed by the fluctuation of the revolving disc using a heterogeneous and homogeneous reactive model. Rasool and Zhang (2019) investigated the flow of Eyring-Powell nanofluid across the Riga plate, as well as the effects of a chemical reaction and thermal radiation.

Several chemical reactions and approximately all biochemical reactions do not work spontaneously and require the smallest quantity of energy to initiate, namely, activation energy. Sajid et al. (2018) investigated the Darcy-Forchheimer flow of a rate-type liquid under the influence of activation energy and radiative heat flux. The activation energy in the flow of cross nano-liquid near a stagnation point was studied by Khan et al. (2018).

Boundary-layer (BL) flows are mainly divided into two dimensionless categories, namely, the similar and nonsimilar flows. Similar solutions have been intensively studied in convective problems. The BL equations served as simplified versions of Navier-Stokes, energy, and concentration equations in the BL region. The transformation of BL equations into another set of ordinary differential equations (ODEs) that can be handled easily with established approaches has resulted in an interesting class of solutions known as similarity solutions, and these transformations are known as similarity transformations. But when such types of similarity do not exist, one has to ultimately determine the solution of the nonlinear PDEs. Considerable mathematical complications are associated with the consequences of the BL equations, mainly because of their nonlinearity. Several approximate numerical and analytical approaches have been developed to solve these BL equations, but before applying these techniques one has to transform the dimensional BL equations into dimensionless form by means of suitable transformations. In most cases the number of independent variables cannot be deduced after employing the transformation, and these equations are termed nonsimilar equations, since at least one of the physical parameters contains a local independent variable. Such BL flows are known as nonsimilar and are practically more realistic. In nonsimilar flows we are forced to nondimensionalize the leading equations through nonsimilarity transformations (Sparrow et al., 1970; Massoudi, 2021; Rasool and Zhang, 2019).

Nonsimilar BL flows are more significant not only theoretically but also have immense implementations. Regardless of this reality, there are few publications in the field of nonsimilar flows. In nonsimilar flows the physical quantities change in the streamwise direction. However, the nonsimilar terms may arise due to the presence of independent variables in some of the dimensionless parameters such as the Eckert number, Grashof number, Weissenberg number, Reynolds number, Deborah number, and magnetic field, which might be a function of coordinate "x" The nonsimilar PDEs can be calculated by operating the method of implicit finite difference, local nonsimilarity (LNS), and the perturbation method.

In this article we have presented nonsimilar solutions for the Eyring-Powell nanofluid model. This research article is organized into three stages. At the first step, Eyring-Powell nanofluid development is discussed in the presence of viscous dissipation, chemical reaction, and heat generation with activation energy over a Riga plate. Suitable nonsimilarity transformations are proposed. The governing convection system is reduced into nondimensional nonlinear PDEs. The second phase demonstrates the influence of distinct parameters, including thermophoresis, Eckert number, Lewis number, Prandtl number, and Brownian motion, on a Riga surface with regard to concentration temperature and velocity profiles. Furthermore, using LNS the transformed system is then resolved analytically and numerically via bvp4c. In the third phase, tabular values of flow, heat, and mass transfer rates are represented.

2. FORCED CONVECTION EQUATIONS

Suppose steady, two-dimensional, Eyring-Powell nanofluid flow above a stretching Riga plate with velocity $u = ax$. We have assumed convective boundary conditions. The Riga plate is heated with the initial temperature T_1 and

concentration C_{np}, where T_∞ is the ambient temperature and h_1 and h_2 are heat and mass transport coefficients, respectively (Nazeer et al., 2020). It is an observation that when Lorentz force is generated with the help of a Riga plate along with the involvement of nanoparticles in the fluid, then the behavior of fluids is electrically conducting with the normal surface. In Fig. 1 the x-axis is chosen near the Riga plate surface the y-axis is normal to that surface. The governing flow equations of the problem are

$$\frac{\partial u}{\partial x}+\frac{\partial v}{\partial y}=0, \tag{1}$$

$$u\frac{\partial u}{\partial x}+v\frac{\partial u}{\partial y}-\left(\nu+\frac{1}{\gamma C\rho_l}\right)\frac{\partial^2 u}{\partial y^2}+\frac{1}{2\gamma C\rho_l^3}\frac{\partial^2 u}{\partial y^2}\left(\frac{\partial u}{\partial y}\right)^2=-\left(\frac{u\nu}{k}-\frac{u^2C_b}{\sqrt{k}}\right)+\frac{J_o\pi M_o}{8\rho_l}e^{(-y\pi/b)}, \tag{2}$$

$$u\frac{\partial T}{\partial x}+v\frac{\partial T}{\partial y}-\tau D_B\left(\frac{\partial C}{\partial y}\frac{\partial T}{\partial y}\right)+\frac{\tau D_T}{T_\infty}\left(\frac{\partial T}{\partial y}\right)^2=\frac{Q_o}{\rho C_p}(T-T_\infty)-\frac{1}{\rho C_p}\frac{\partial q_r}{\partial y}+\frac{\nu}{\rho C_p}\left(\frac{\partial u}{\partial y}\right)^2+\alpha\left(\frac{\partial^2 T}{\partial y^2}\right), \tag{3}$$

$$u\frac{\partial C}{\partial x}+v\frac{\partial C}{\partial y}=D_B\left(\frac{\partial^2 C}{\partial y^2}\right)-(C-C_\infty)\left(K_r^2\left(\frac{T}{T_\infty}\right)^n\exp\left(\frac{-E_a}{Tk}\right)+K\right)+\frac{D_T}{T_\infty}\left(\frac{\partial^2 T}{\partial y^2}\right). \tag{4}$$

The boundary conditions for a given problem are

$$\begin{aligned}&\text{at}\quad y=0,\quad u=ax-k\frac{\partial T}{\partial y}=h_1(T_1-T),\quad \left(\frac{\partial C}{\partial y}\right)-h_2(C-C_{np})=0,\quad v=0\\&\text{as}\quad y\to\infty,\quad u\to 0,\quad C\to C_\infty,\quad T\to T_\infty.\end{aligned} \tag{5}$$

The radiative heat flux q_r is defined as

$$q_r=-\frac{4\sigma^\circ}{3k^\circ}\left(\frac{\partial T^4}{\partial y}\right). \tag{6}$$

By making use of Taylor series expansion,

$$T^4=T_\infty^4+4T_\infty^3(T-T_\infty)+6T_\infty^2(T-T_\infty)^2+\ldots.$$

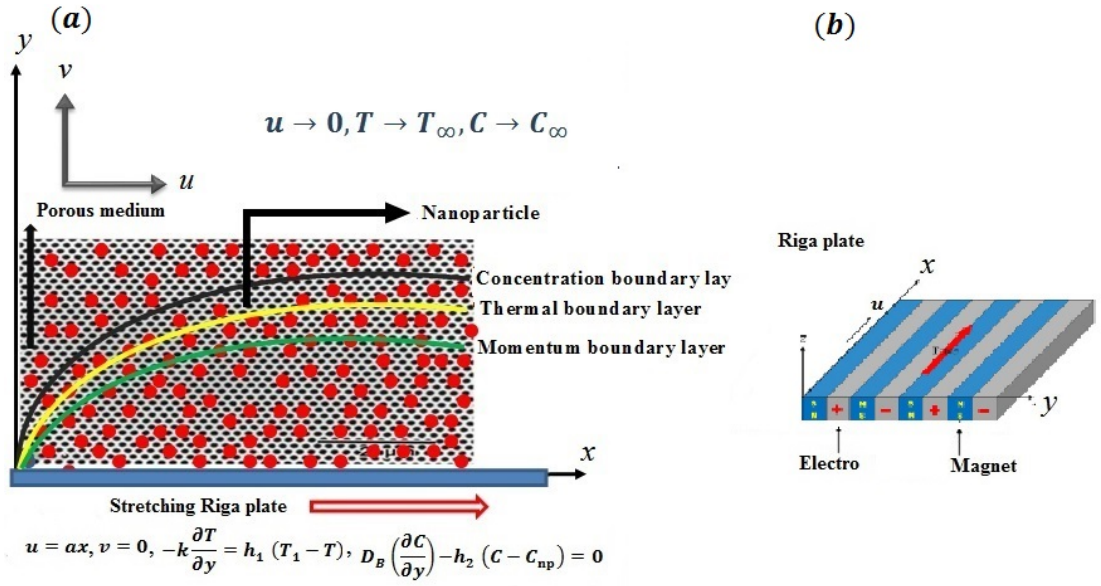

FIG. 1: (a) Flow configuration and (b) Lorentz force induced Riga plate

After neglecting higher-order terms in the above equation, we get Eq. (7).
By utilization of Eq. (7) in Eq. (3), we obtain Eq. (8) as given below:

$$q_r = -\frac{16T_\infty^3 \sigma^\circ}{3k^\circ}\left(\frac{\partial T}{\partial y}\right), \tag{7}$$

$$\begin{aligned} u\frac{\partial T}{\partial x} + v\frac{\partial T}{\partial y} - \alpha\left(\frac{\partial^2 T}{\partial y^2}\right) - \frac{(\rho C)_p}{(\rho C)_l}\left(D_B \frac{\partial C}{\partial y}\frac{\partial T}{\partial y}\right) = \frac{Q_o}{\rho C_p}(T - T_\infty) + \frac{16T_\infty^3 \sigma^\circ}{3K^\circ (\rho C)_l}\frac{\partial^2 T}{\partial y^2} \\ - \frac{\nu}{\rho C_p}\left(\frac{\partial u}{\partial y}\right)^2 + \frac{(\rho C)_p}{(\rho C)_l}\frac{D_T}{T_\infty}\left(\frac{\partial T}{\partial y}\right)^2. \end{aligned} \tag{8}$$

3. NONSIMILAR SYSTEM

Considering the nonsimilar flow, we have introduced new parameters $\xi(x)$ as a nonsimilarity variable and $\eta(xy)$ as a pseudosimilarity variable (Cui et al., 2021a; Razzaq et al., 2021):

$$\begin{aligned} &\xi = \frac{x}{l}, \quad \eta = \sqrt{\frac{a}{\nu}}y, \quad u = ax\frac{\partial f}{\partial \eta}(\xi,\eta), \quad v = -\sqrt{a\nu}\left(\xi\frac{\partial f}{\partial \xi} + f(\xi,\eta)\right) \\ &\phi(\xi,\eta) = \frac{C - C_\infty}{(C_{np} - \mathrm{C}_\infty)}, \quad \theta(\xi,\eta) = \frac{T - T_\infty}{(T_1 - T_\infty)}. \end{aligned} \tag{9}$$

Using Eq. (9) in Eqs. (2), (3), and (8), we get the following dimensionless system:

$$\begin{aligned} &\frac{\partial^3 f}{\partial \eta^3}\left(1 + K - K\xi^2\lambda\left(\frac{\partial^2 f}{\partial \eta^2}\right)^2\right) + Q\xi^{-1}\exp(-\eta\beta) - D_1\frac{\partial f}{\partial \eta} - D_2\xi\left(\frac{\partial f}{\partial \eta}\right)^2 - \left(\frac{\partial f}{\partial \eta}\right)^2 \\ &+ f\frac{\partial^2 f}{\partial \eta^2} = \xi\left(\frac{\partial f}{\partial \eta}\frac{\partial^2 f}{\partial \xi \partial \eta} - \frac{\partial^2 f}{\partial \eta^2}\frac{\partial f}{\partial \xi}\right), \end{aligned} \tag{10}$$

$$\begin{aligned} &\left(1 + \frac{4}{3}Rd\right)\frac{\partial^2 \theta}{\partial \eta^2} + \mathrm{Pr}\left(f\frac{\partial \theta}{\partial \eta} + N_b\frac{\partial \theta}{\partial \eta}\frac{\partial \phi}{\partial \eta} + N_t\left(\frac{\partial \theta}{\partial \eta}\right)^2 + \xi^2 \mathrm{Ec}\left(\frac{\partial^2 f}{\partial \eta^2}\right)^2 + q\theta\right) \\ &= \mathrm{Pr}\xi\left(\frac{\partial f}{\partial \eta}\frac{\partial \theta}{\partial \xi} - \frac{\partial \theta}{\partial \eta}\frac{\partial f}{\partial \xi}\right), \end{aligned} \tag{11}$$

$$\frac{\partial^2 \phi}{\partial \eta^2} + \frac{N_t}{N_b}\frac{\partial^2 \theta}{\partial \eta^2} + \mathrm{Sc}\, f\frac{\partial \phi}{\partial \eta} - K_1 \mathrm{Sc}\,\phi - \sigma \mathrm{Sc}\,\phi(1 + \theta\delta)^n \exp\frac{-E}{(1 + \theta\delta)} = \xi \mathrm{Sc}\left(\frac{\partial f}{\partial \eta}\frac{\partial \phi}{\partial \xi} - \frac{\partial \phi}{\partial \eta}\frac{\partial f}{\partial \xi}\right). \tag{12}$$

Subjected boundary conditions:

$$\begin{aligned} &\frac{\partial f(\xi,0)}{\partial \eta} = 1, \quad f(\xi,0) + \xi\frac{\partial f(\xi,0)}{\partial \xi} = 0, \quad \frac{\partial \theta(\xi,0)}{\partial \eta} = -\alpha_1(1 - \theta(\xi,0)) \\ &\frac{\partial \phi(\xi,0)}{\partial \eta} = -\alpha_2(1 - \theta(\xi,0)), \quad \frac{\partial f(\xi,\infty)}{\partial \eta} \to 0, \quad \theta(\xi,\infty) \to 0, \quad \phi(\xi,\infty) \to 0. \end{aligned} \tag{13}$$

Here $\beta = \sqrt{\nu/a}\,(\pi/b)$ is a dimensionless number, $N_t = [\tau(T_1 - T_\infty)D_T]/(\nu T_\infty)$ is the thermophoresis parameter, $E = -E_a/(kT_\infty)$ is activation energy, $Q = (J_o \pi M_o)/(8l\,a^2\rho_l)$ modifies the form of Hartmann number, $Rd = (16T_\infty^3\sigma^\circ)/(3kK^*)$ is the radiation parameter, $\alpha_1 = (h_1/k)\sqrt{\nu/\mathrm{a}}$, $\alpha_2 = (h_2/k)\sqrt{\nu/a}$ the heat–mass transport Biot factor, $\mathrm{Pr} = \nu/\alpha$ is the Prandtl number, $\lambda = (a^3 l^2 \rho_l)/(2\nu C^2)$ and $K = 1/(C\nu\gamma)$ are fluid parameters, $N_b = [\tau(C_{np} - C_\infty)D_B]/(\nu T_\infty)$, $1/\mathrm{Sc} = D_B/\nu$ are Brownian motion and Schmidt number, and $D_1 = \nu/ak$, $D_2 = lC_b/\sqrt{k}$ is used for the dimensionless porous medium. $\mathrm{Ec} = U_o^2/[C_p(T_1 - T_\infty)\rho]$, $\delta = (T_1 - T_\infty)/T_\infty$,

$K_1 = K/a$, $\sigma = K_r^2/a$, and $q = Q_o/(a\rho C_p)$ are the Eckert number, temperature difference variable, chemical reaction, and heat source/sink, respectively. The important physical parameters, namely, skin friction, Nusselt number, and Sherwood number, are given below:

$$\begin{aligned} &\mathrm{Re}^{1/2}C_f = (1+K)\,f''(\xi,0) - \frac{K}{3}\lambda\xi^2 f''^3(\xi,0), \quad \mathrm{Re}^{-1/2}\mathrm{Nu} = \left(1+\frac{4}{3}Rd\right)\theta'(\xi,0) \\ &\mathrm{Re}^{-1/2}\mathrm{Sh} = -\phi'(\xi,0), \end{aligned} \tag{14}$$

where $\mathrm{Re} = al^2/\nu$.

LNS is a frequently used technique for nonsimilar BL problems. It is very helpful to evaluate the local similarity technique before proceeding further to local nonsimilar solutions. According to this method, the right-hand side term $\partial(.)/\partial\xi$ of Eqs. (10)–(12) are determined to be appropriately small and thus can be approximated to zero, assuming a structure of BL equations with the following conditions:

$$\frac{\partial^3 f}{\partial\eta^3}\left(1+K-K\xi^2\lambda\left(\frac{\partial^2 f}{\partial\eta^2}\right)^2\right) + Q\xi^{-1}\exp(-\eta\beta) - D_1\frac{\partial f}{\partial\eta} - D_2\xi\left(\frac{\partial f}{\partial\eta}\right)^2 - \left(\frac{\partial f}{\partial\eta}\right)^2 + f\frac{\partial^2 f}{\partial\eta^2} = 0, \tag{15}$$

$$\left(1+\frac{4}{3}Rd\right)\frac{\partial^2\theta}{\partial\eta^2} + \mathrm{Pr}\left(f\frac{\partial\theta}{\partial\eta} + N_b\frac{\partial\theta}{\partial\eta}\frac{\partial\phi}{\partial\eta} + N_t\left(\frac{\partial\theta}{\partial\eta}\right)^2 + \xi^2\mathrm{Ec}\left(\frac{\partial^2 f}{\partial\eta^2}\right)^2 + q\theta\right) = 0, \tag{16}$$

$$\frac{\partial^2\phi}{\partial\eta^2} + \frac{N_t}{N_b}\frac{\partial^2\theta}{\partial\eta^2} + \mathrm{Sc}\,f\frac{\partial\phi}{\partial\eta} - K_1\mathrm{Sc}\,\phi - \sigma\mathrm{Sc}\phi(1+\theta\delta)^n\exp\frac{-E}{(1+\theta\delta)} = 0, \tag{17}$$

$$\begin{aligned} &\frac{\partial f(\xi,0)}{\partial\eta} = 1, \quad f(\xi,0) = 0, \quad \frac{\partial\theta(\xi,0)}{\partial\eta} = -\alpha_1(1-\theta(\xi,0)) \\ &\frac{\partial\phi(\xi,0)}{\partial\eta} = -\alpha_2(1-\phi(\xi,0)), \quad \frac{\partial f(\xi,\infty)}{\partial\eta} \to 0, \quad \theta(\xi,\infty)\to 0, \quad \phi(\xi,\infty)\to 0. \end{aligned} \tag{18}$$

At any streamwise location, the quantity ξ may be considered as a constant parameter. Thus the above-mentioned equations (15)–(18) can be treated as ODEs. It should be noted that the ignorance of terms $\partial(.)/\partial\xi$ creates some dubious results. To overcome these challenges, Sparrow et al. (1970) and Sparrow and Yu (1971) proposed a LNS approach for obtaining the nonsimilar BL equations consequences.

Making use of a LNS method, let us introduce the functions

$$\begin{aligned} &\frac{\partial f}{\partial\eta} = f', \quad \frac{\partial^2 f}{\partial\eta^2} = f''\frac{\partial^3 f}{\partial\eta^3} = f''', \quad \frac{\partial\theta}{\partial\eta} = \theta', \quad \frac{\partial^2\theta}{\partial\eta^2} = \theta'', \quad \frac{\partial\phi}{\partial\eta} = \phi\frac{\partial^2\phi}{\partial\eta^2} = \phi'' \\ &g(\xi,\eta) = \frac{\partial f(\xi,\eta)}{\partial\xi}, \quad s(\xi,\eta) = \frac{\partial\theta(\xi,\eta)}{\partial\xi}, \quad w(\xi,\eta) = \frac{\partial\phi(\xi,\eta)}{\partial\xi}. \end{aligned} \tag{19}$$

Now by using Eq. (19) in Eqs. (8)–(11), the equations are transformed as

$$f'''\left(1+K-K\xi^2\lambda f''^2\right) + Q\xi^{-1}\exp(-\eta\beta) - D_1 f' - D_2\xi f'^2 + f''f = \xi(f'g' - f''g), \tag{20}$$

$$\left(1+\frac{4}{3}Rd\right)\theta'' + \mathrm{Pr}\left(N_b\theta'\phi' + N_t\theta'^2 + \theta' f + q\theta + \xi^2\mathrm{Ec}\,f''^2 + q\theta\right) = \mathrm{Pr}\,\xi(f's - \theta' g), \tag{21}$$

$$\phi'' + \frac{N_t}{N_b}\theta'' + \mathrm{Sc}\,f\phi' - K_1\mathrm{Sc}\,\phi - \sigma\mathrm{Sc}\,\phi(1+\theta\delta)^n\exp\frac{-E}{(1+\theta\delta)} = \xi\mathrm{Sc}\,(f'w - \phi' g), \tag{22}$$

$$\begin{aligned} &f'(\xi,0) = 1, \quad f(\xi,0) + \xi g(\xi,0) = 0, \quad \theta'(\xi,0) = -\alpha_1(1-\theta(\xi,0)) \\ &\phi'(\xi,0) = -\alpha_2(1-\phi(\xi,0)), \quad f'(\xi,\infty)\to 0, \quad \theta(\xi,\infty)\to 0, \quad \phi(\xi,\infty)\to 0. \end{aligned} \tag{23}$$

We get Eqs. (24)–(27) by taking partial derivatives of Eqs. (19)–(22) with respect to ξ:

$$f'''\left(1+K-K\xi^2\lambda f''^2\right)-2\xi K\lambda f'''\left(f''^2+\xi g''f''\right)-Q\xi^{-2}\exp\left(-\eta\beta\right)-D_1g'-D_2f'^2-D_2\xi f'^2 \\ -2D_2\xi f'g'-3f'g'+2f''g+g''f=\xi\left(g'^2-g''g\right), \tag{24}$$

$$\left(1+\frac{4}{3}Rd\right)s''+\mathrm{Pr}\left(N_bs'\phi'+N_bw'\phi'+2N_t\theta's'+2\xi\mathrm{Ec}\,f''^2+2\xi^2\mathrm{Ec}\,f''g''+qs+2\theta'g-f's+s'f\right) \\ =\mathrm{Pr}\,\xi\left(g's-s'g\right), \tag{25}$$

$$\phi''-\sigma\mathrm{Sc}\left(ns\delta\,(1+\theta\delta)^{n-1}\exp\frac{-E}{(1+\theta\delta)}\,\phi-(1+\theta\delta)^{n-2}\exp\frac{-E}{(1+\theta\delta)}\,\phi\delta s\right)+\frac{N_t}{N_b}s''+2\mathrm{Sc}\,g\phi' \\ -K_1\mathrm{Sc}\,w-(1+\theta\delta)^n\exp\frac{-E}{(1+\theta\delta)}\,w=\xi\mathrm{Sc}\left(g'w-w'g\right), \tag{26}$$

$$g\left(\xi,0\right)=0,\quad g'\left(\xi,0\right)=0,\quad s'\left(\xi,0\right)=\alpha_1s\left(\xi,0\right),\quad w'\left(\xi,0\right)=\alpha_2w\left(\xi,0\right),\quad g'\left(\xi,\infty\right)\to0 \\ s\left(\xi,\infty\right)\to0,\quad w\left(\xi,\infty\right)\to0. \tag{27}$$

4. NUMERICAL SOLUTION

This section demonstrates the impacts of various parameters on convective heat transfer. Here, the LNS technique is applied to transform the system of Eqs. (10)–(13) into the system of ODEs. Then this system of ODEs is tackled by means of bvp4c (built-in Matlab algorithm). bvp4c is a Matlab tool that uses a three-stage Labatto III code to do finite difference calculations. The numerical simulation error is approximated in bvp4c using the residual error module. The graphical simulations and tabular data given in this study passed the bvp4c tolerance criteria. The influences of the dimensionless parameter of the porous medium D_1, D_2 on velocity profiles are drawn in Figs. 2 and 3. It has an important effect on flow motion. Generally, the hindrance in the flow path is because of porosity, which demonstrates that velocity has decreasing behavior. In fact, when the value of D_1 increases, the number of holes is enhanced, which creates a disturbance in the flow motion. Therefore it is obvious that for increased values of D_1, decreasing behavior is exhibited by the velocity profile. The influence of the nondimensional parameter β is demonstrated in Fig. 4. By increasing values of β the viscosity increases, hence declining the behavior of the flow pattern. Illustration of fluid parameter K on the velocity field is shown in Fig. 5. Clearly, the velocity profile decays for parameter K. Figure 6

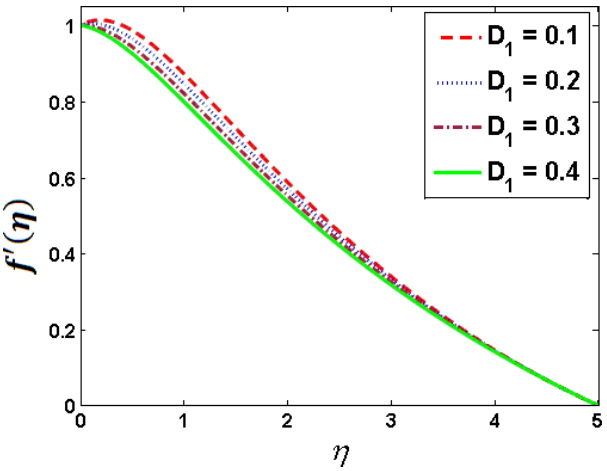

FIG. 2: Variation of D_1 vs. $f'(\eta)$

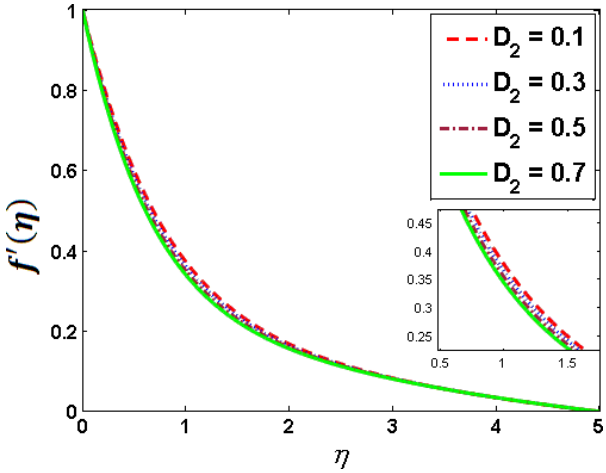

FIG. 3: Variation of D_2 vs. $f'(\eta)$

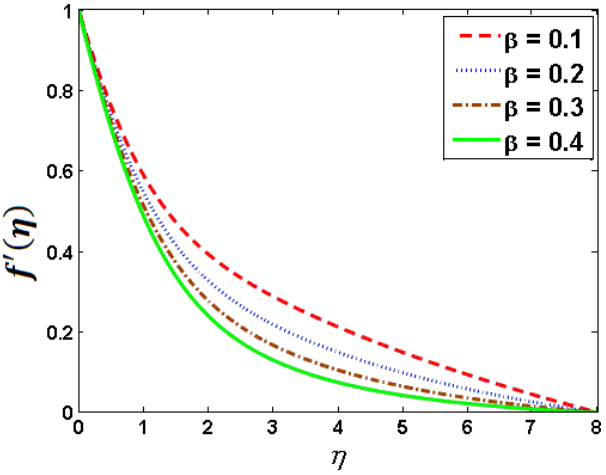

FIG. 4: Variation of β vs. $f'(\eta)$

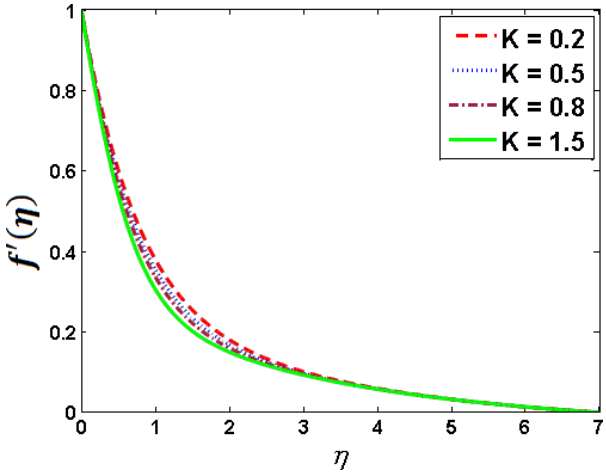

FIG. 5: Variation of K vs. $f'(\eta)$

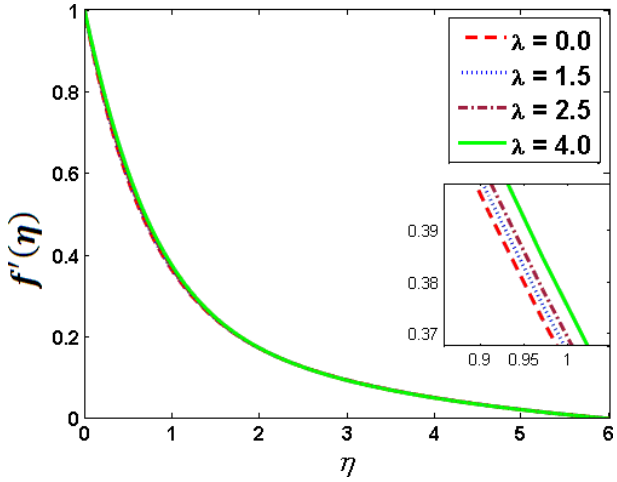

FIG. 6: Variation of λ vs. $f'(\eta)$

demonstrates the distribution of $f'(\eta)$ for different values of λ. The velocity $f'(\eta)$ and boundary-layer thickness is a rising function of λ. For higher values of Ec, viscous dissipation increases therefore temperature increases by increasing Eckert number, as shown in Fig. 7. It is noted that the concentration profile decreases by increasing the Eckert number. The temperature profile shows increasing behavior for increasing values of α_1. This is because of the associated BL for the higher values of α_1 (Rasool and Zhang, 2019; Nazeer et al., 2020).

An illustration of α_2 on temperature is described in Fig. 8. Mass convection increases by increasing the values of α_2. The temperature configuration under the influences of Brownian motion N_b is shown in Fig. 9. Clearly, temperature increases by increasing N_b, and also the thickness of the thermal boundary layer is enhanced. By increasing the values of N_b, the motion of the particles increases, which produces more heat. Therefore an increase in the temperature profile is noticed. The behavior of N_t versus temperature is shown in Fig. 10. This shows that growth in N_t increases in the thermal BL. The temperature is exhibited in Fig. 11 biased by momentum to mass diffusivity ratio, descending conduct is observed toward augmented values of the used parameter, i.e., Pr.

The concentration profile vs the Eckert number is demonstrated via Fig. 12. Clearly, the concentration profile decreases when the values of the Eckert number increase. We analyzed the concentration profile in Fig. 13 for different values of σ, which illustrates that concentration decays for higher estimations of σ. Figure 14 displays the effects of

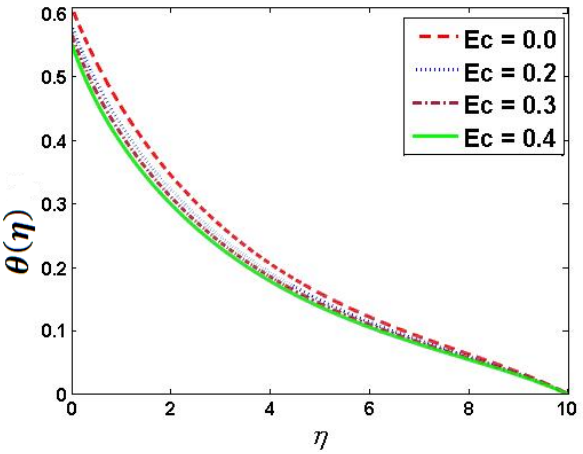

FIG. 7: Variation of Ec vs. θ(η)

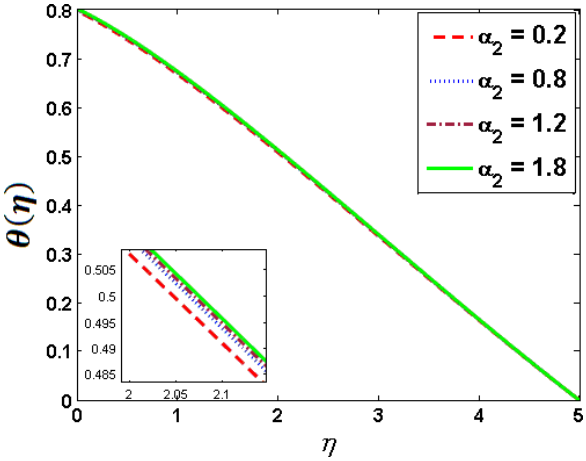

FIG. 8: Variation of α_2 vs. θ(η)

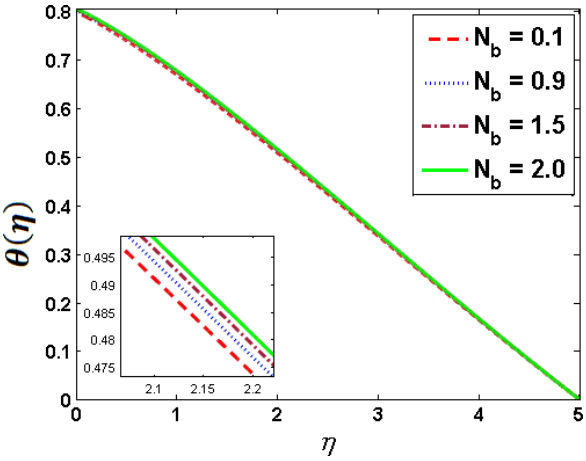

FIG. 9: Variation of N_b vs. θ(η)

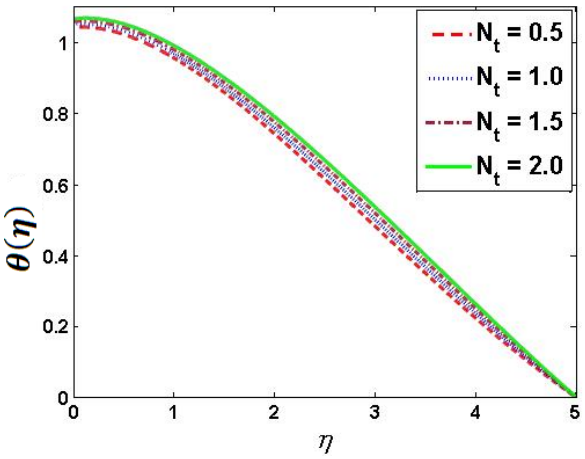

FIG. 10: Variation of N_t vs. θ(η)

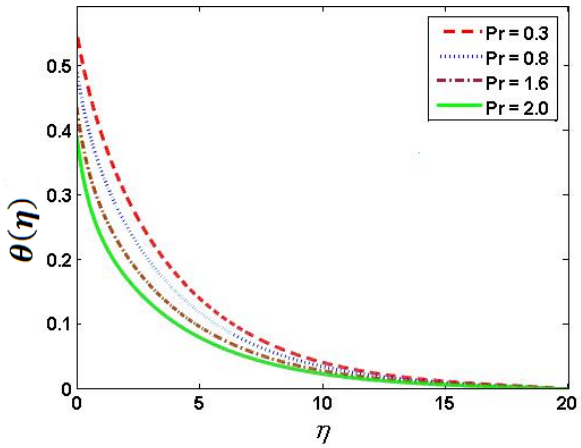

FIG. 11: Variation of Pr vs. θ(η)

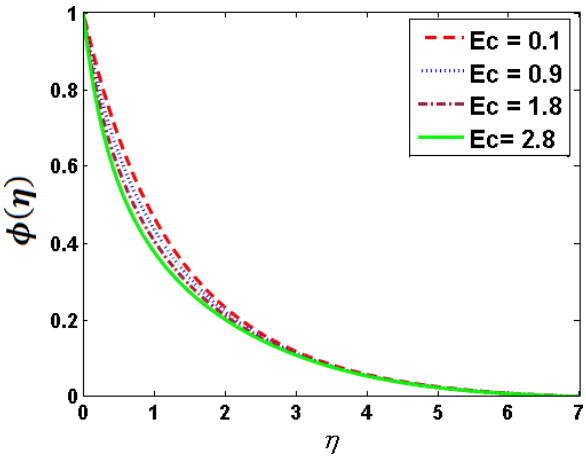

FIG. 12: Variation of Ec vs. ϕ (η)

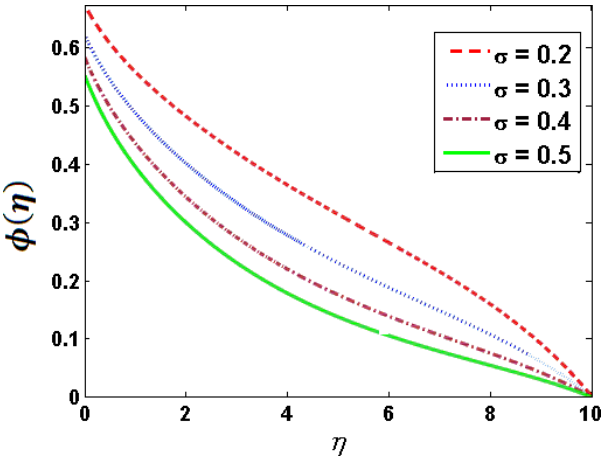

FIG. 13: Variation of σ vs. ϕ (η)

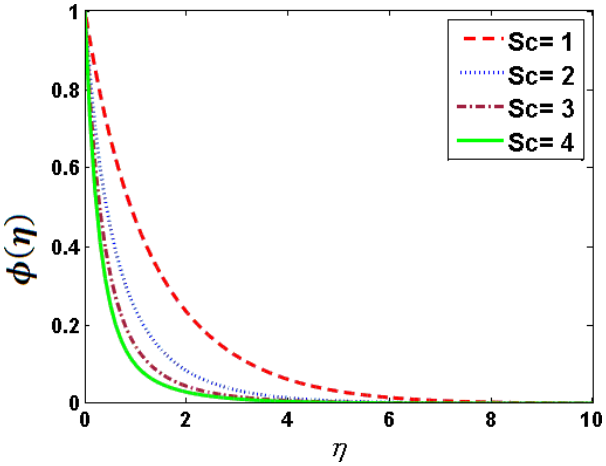

FIG. 14: Variation of Sc vs. ϕ (η)

Sc on the concentration of nanoparticles; for the higher value of Sc, ϕ (η) is reducing. The Schmidt number is a product of the Lewis and Prandtl numbers. The increase in Lewis number indicates a wide thermal diffusivity that is a reaction to low heat capacity and higher thermal conductivity.

The concentration profile's behavior versus fluid parameter K is depicted in Fig. 15. The concentration profile decreases for increased values of K because of scattering among the fluid's particles toward the surface, and therefore the corresponding BL decreases.

Table 1 describes the range of dimensionless numbers for which the numerical scheme provides convergent solutions. Tables 2–4 reveal the comparison of local similar friction, heat, and mass transfer rates of Nazeer et al. (2020) with present nonsimilar consequences. Comparisons between similar and nonsimilar flows were presented by Cui et al. (2021b) and Razzaq and Farooq (2021).

Table 2 contains the numerical description of various parameters. It is explored that the drag force is enhanced for rising values of β; however, a reverse trait is expressed versus Q and K. The outcomes of Sh and Nu for numerous parameters are expressed in Tables 3 and 4. Here the heat transmission rates show the expansion via D_1, q, Ec, and Rd while the opposite is shown for Pr. Additionally, the values of Sh predict the contraction via D_1, q, Rd, and Ec, while code validation for the coefficient of skin friction is described in Table 5.

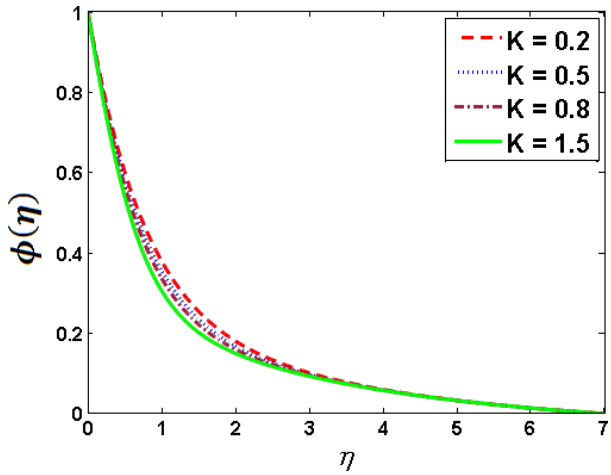

FIG. 15: Variation of K vs. ϕ (η)

TABLE 1: Range table for a stable solution

β	Rd	D_2	Ec	K	N_t	Pr	N_b	Q	α_1	α_2
0.1–140	0.5	0.5	0.4	0.1	0.5	6.2	0.1	0.3	0.5	1
0.5	**0.1–1**	0.5	0.4	0.1	0.5	6.2	0.1	0.3	0.5	1
0.5	0.5	**0.1–80**	0.4	0.1	0.5	6.2	0.1	0.3	0.5	1
0.5	0.5	0.5	**0.1–8**	0.1	0.5	6.2	0.1	0.3	0.5	1
0.5	0.5	0.5	0.4	**0.1–3**	0.1–1	6.2	0.1	0.3	0.5	1
0.5	0.5	0.5	0.4	0.1	0.5	**6.2–30**	0.1	0.3	0.5	1
0.5	0.5	0.5	0.4	0.1	0.5	6.2	**0.1–1**	**0.1–15**	0.5	1
0.5	0.5	0.5	0.4	0.1	0.5	6.2	0.1	0.3	**0.1–2**	1
0.5	0.5	0.5	0.4	0.1	0.5	6.2	0.1	0.3	0.5	**0.1–2**

TABLE 2: Variation of $C_{fx}(\mathrm{Re}_x^{1/2})$ for dimensionless parameters β, Q, K, when $q = Rd = 0.3$, $D_1 = D_2 = K_2 = 0.2$, $\delta = 0.8$, Ec $= 4$, $\sigma = 0.8$, $n = 0.9$, $E = \alpha_1 = \alpha_2 = \lambda = \xi = 1$, $N_b = K_1 = 0.1$, $N_t = 0.7$, Pr $= 0.5$, Le $= 0.4$

Parameters			$C_{fx}(\mathrm{Re}_x^{1/2})$			
K	β	Q	**Nazeer et al. (2020)**	**Present Study**		**Difference (%)**
				Local Similar Case	**Nonsimilar Case**	
0.0	1.1	0.3	1.1434	1.0217133319	0.9676393399	5.292481786
0.5	1.1	0.3	0.9723	1.4282756818	1.3241858691	7.287795628
1.0	1.1	0.3	0.8592	1.7818150208	1.6016167802	10.11318451
0.3	**0.0**	0.3	0.9282	1.1180576074	0.5675870515	49.23454322
0.3	**0.5**	0.3	0.9909	1.2197831005	0.8874581724	27.24459192
0.3	**1.0**	0.3	1.0267	1.2678631280	1.1739609614	7.406333107
0.3	1.1	**0.0**	1.1412	1.3849286147	1.5553499567	12.30542428
0.3	1.1	**0.5**	0.9607	1.1920389284	1.2334382888	3.472987284
0.3	1.1	**1.0**	0.7866	0.9586677635	1.0592589492	10.49280987

5. CONCLUSION

The current study analyzed the impacts of heat generation, activation energy, porous medium, thermal radiation, and chemical reaction on Eyring-Powell nanofluid flow over a Riga plate. The analysis shows the following:

- Velocity decreases for increasing estimations of the magnetic field.
- The temperature enhances for higher Prandtl number but decreasing behavior occurs for heat generation and radiation parameters.
- The enhanced K estimations reduced the nanoparticle concentration close to the radiative Riga plate.
- Concentration and temperature decrease for rising values of the fluid parameter.
- The temperature decays via modified Hartman number.
- Temperature and concentration profiles decrease versus higher estimations of Eckert number.

TABLE 3: Variation of $\mathrm{Nu}(\mathrm{Re}_x^{-1/2})$ for distinct values of Rd, Ec, K, D_1, when $q = 0.3$, $D_2 = K_2 = 0.2$, $\delta = 0.8$, $\sigma = 0.8$, $n = 0.9$, $E = \lambda = \xi = \alpha_1 = \alpha_2 = 1$, $N_b = K_1 = 0.1$, $N_t = 0.7$, $\mathrm{Le} = 0.4$, $\beta = 1.1$

Parameters					$\mathrm{Nu}(\mathrm{Re}_x^{-1/2})$		
D_1	q	Ec	Rd	Nazeer et al. (2020)	Present Study		Difference (%)
					Local Similar Case	Nonsimilar Case	
0.3	0.5	0.2	0.3	0.7876	0.1629731030	0.2084513334	27.90535957
0.4	**0.1**	0.2	0.3	0.7895	0.1610808277	0.2062265006	28.02672022
0.5	**0.2**	**0.4**	0.3	0.7913	0.1596251316	0.2042512256	27.95680953
0.2	**0.4**	**0.5**	**0.4**	0.7639	0.2175418270	0.2434602529	11.91422645
0.2	0.3	**0.6**	**0.5**	0.7691	0.1837537632	0.2277182889	23.92578249
0.6	0.5	0.2	**0.6**	0.7800	0.0986030182	0.1929727812	95.70676915
—	—	—	—	0.7914	0.1917448468	0.2024710461	5.593996125
—	—	—	—	0.8003	0.1864779746	0.1982392382	6.307052415
—	—	—	—	0.8095	0.1812135335	0.1940064814	7.059598504
—	—	—	—	0.8360	0.2796792800	−0.1693253894	160.5427007
—	—	—	—	0.9156	0.3957035598	0.0516789164	86.93999204
—	—	—	—	0.9954	0.5094866286	0.2110329498	58.57929572

TABLE 4: Variation of Sherwood number $\mathrm{Sh}(\mathrm{Re}_x^{-1/2})$ for distinct Rd, Ec, K, D_1, when $q = 0.3$, $D_2 = K_2 = 0.2$, $\delta = 0.8$, $\sigma = 0.8$, $n = 0.9$, $E = \lambda = \xi = \alpha_1 = \alpha_2 = 1$, $N_b = K_1 = 0.1$, $N_t = 0.7$, $\mathrm{Le} = 0.4$, $\beta = 1.1$

Parameters					$\mathrm{Sh}(\mathrm{Re}_x^{-1/2})$		
D_1	q	Ec	Rd	Nazeer et al. (2020)	Present Study		Difference (%)
					Local Similar Case	Nonsimilar Case	
0.3	0.5	0.2	0.3	0.2130	2.3910058017	0.1224944888	94.87686359
0.4	0.1	0.2	0.3	0.2128	2.4495521407	0.1404935202	94.26452216
0.5	0.2	0.4	0.3	0.2127	2.5051589961	0.1564650189	93.75428789
0.2	0.4	0.5	0.4	0.2171	0.4151120735	0.1328868101	67.98772703
0.2	0.3	0.6	0.5	0.2162	0.8507545902	0.1886923133	77.82059416
0.6	0.5	0.2	0.6	0.2141	1.8049396797	0.2309959526	87.20201261
—	—	—	—	0.2120	1.6305674618	0.3951404343	75.76669205
—	—	—	—	0.2104	1.7891354999	0.4362826288	75.61489173
—	—	—	—	0.2088	1.9476209970	0.4774914507	75.48334859
—	—	—	—	0.1980	2.5641755737	0.4551284442	82.25049607
—	—	—	—	0.1978	2.5929238138	0.4669403908	81.99174275
—	—	—	—	0.1977	2.6324567328	0.4788274602	81.81062373

TABLE 5: Code validation. Coefficient of skin friction when $D_2 = 1$, $K = \beta = Q = D_1 = 0$

Parameter	For $\xi = 0$			For $\xi = 1$	
	Ibrahim and Negera (2020)	Ittedi et al. (2017)	Present Result	Cui et al. (2021a)	Present Result
$M = 0.0$	1.2105	1.2105	1.21052	1.28141466	1.2843131024

- Temperature decays for increasing values of the heat source parameter $q > 0$ while it is enhanced for heat sink parameters $q < 0$.
- A boost in radiation expands the thermal boundary layer.
- Enhancement of D_1, q, Ec, Rd leads to an increase in Sherwood number.

ACKNOWLEDGMENTS

This work was supported by the National Natural Science Foundation of China (Approval Nos. 12062018 and 12172333), Program for Young Talents of Science and Technology in Universities of Inner Mongolia Autonomous Region (Approval No. NJYT22075), and the Natural Science Foundation of Inner Mongolia (Approval No. 2020MS01015).

The authors declare there is no conflict of interest.

REFERENCES

Abid, M., Khan, M.S., Ratlamwala, T.A.H., Malik, M.N., Ali, H.M., and Cheok, Q., Thermodynamic Analysis and Comparison of Different Absorption Cycles Driven by Evacuated Tube Solar Collector Utilizing Hybrid Nanofluids, *Energy Convers. Manage.*, vol. **246**, p. 114673, 2021.

Akbar, N.S., Ebaid, A., and Khan, Z.H., Numerical Analysis of Magnetic Field Effects on Eyring-Powell Fluid Flow towards a Stretching Sheet, *J. Magn. Magn. Mater.*, vol. **382**, pp. 355–358, 2015.

Ali, M.H., A Semi-Empirical Model for Retained Condensate on Horizontal Pin-Fin Tube Including the Effect of Vapour Velocity, *Case Studies Therm. Eng.*, vol. **28**, p. 101420, 2021.

Buongiorno, J., Convective Transport in Nanofluids, *J. Heat Transf.*, vol. **128**, no. 3, pp. 240–250, 2006.

Choi, S.U.S., Enhancing Thermal Conductivity of Fluid with Nanoparticles, in Development and Applications of Non-Newtonian Flow, ASME, FED-vol. **231**/MD-vol. **66**, pp. 99–105, 1995.

Cui, J., Razzaq, R., Farooq, U., Khan, W.A., Farooq, F.B., and Muhammad, T., Impact of Non-Similar Modeling for Forced Convection Analysis of Nano-Fluid Flow over Stretching Sheet with Chemical Reaction and Heat Generation, *Alexandria Eng. J.*, vol. **61**, no. 6, pp. 4253–4261, 2021a.

Cui, J., Farooq, U., Razzaq, R., Khan, W.A., and Yousif, M.A., Closure to "Computational Analysis for Mixed Convective Flows of Viscous Fluids with Nanoparticles," *J. Therm. Sci. Eng. Appl.*, vol. **13**, no. 6, Article ID 066001, 2021b.

Das, K., Putra, N., Thiesen, P., and Roetzel, W., Temperature Dependence of Thermal Conductivity Enhancement for Nanofluid, *Trans. ASME J. Heat Transf.*, vol. **125**, no. 4, pp. 567–574, 2003.

Das, S.K., Choi, S.U.S., and Patel, H.E., Heat Transfer in Nanofluid, *Heat Transf. Eng.*, vol. **27**, no. 10, pp. 3–19, 2006.

Eldabe, N.T.M., Hassan, A.A., and Mohamed, M.A.A., Effect of Couple Stresses on the MHD of a Non-Newtonian Unsteady Flow between Two Parallel Porous Plates, *Z. Naturforsch.*, vol. **58**, pp. 204–210, 2003.

Ghadikolaei, S.S., Hosseinzadeh, K., and Ganji, D.D., Analysis of Unsteady MHD Eyring-Powell Squeezing Flow in Stretching Channel with Considering Thermal Radiation and Joule Heating Effect Using AGM, *Case Studies Therm. Eng.*, vol. **10**, pp. 579–594, 2017.

Ghalambaz, M., Groşan, T., and Pop, I., Mixed Convection Boundary Layer Flow and Heat Transfer over a Vertical Plate Embedded in a Porous Medium Filled with a Suspension of Nano-Encapsulated Phase Change Materials, *J. Mol. Liq.*, vol. **293**, p. 111432, 2019.

Ghalambaz, M., Mehryan, S.A.M., Hajjar, A., and Veismoradi, A., Unsteady Natural Convection Flow of a Suspension Comprising Nano-Encapsulated Phase Change Materials (NEPCMs) in a Porous Medium, *Adv. Powder Technol.*, vol. **31**, no. 3, pp. 954–966, 2020.

Gholinia, G., Hosseinzadeh, K., Mehrzadi, M., Ganji, D.D., and Ranjbar, A. A., Investigation of MHD Eyring-Powell Fluid Flow over a Rotating Disk under Effect of Homogeneous Heterogeneous Reactions, *Case Studies Therm. Eng.*, vol. **13**, p. 100356, 2013.

Hayat, T., Abbas, T., Ayub, M., Farooq, M., and Alsaedi, A., Flow of Nanofluid Due to Convectively Heated Riga Plate with Variable Thickness, *J. Mol. Liq.*, vol. **222**, pp. 854–862, 2016.

Hayat, T., Gull, N., Farooq, M., and Ahmad, B., Thermal Radiation Effect in MHD Flow of Powell-Eyring Fluid by a Stretching Cylinder, with Newtonian Heating, *Therm. Sci.*, vol. **22**, pp. 371–382, 2018.

Ibrahim, W. and Negera, M., MHD Slip Flow of Upper-Convected Maxwell Nanofluid over a Stretching Sheet with Chemical Reaction, *J. Egypt. Math. Soc.*, vol. **28**, no. 1, pp. 1–28, 2020.

Ittedi, S., Ramya, D., and Joga, S., MHD Heat Transfer of Nanofluids over a Stretching Sheet with Slip Effects and Chemical Reaction, *Int. J. Latest Eng. Res. Appl.*, pp. 10–20, 2017.

Javed, T., Ali, N., Abbas, Z., and Sajid, M., Flow of an Eyring-Powell Non-Newtonian Fluid over a Stretching Sheet, *Chem. Eng. Commun.*, vol. **200**, pp. 327–336, 2013.

Khan, M.I., Hayat, T., Khan, M.I., and Alsaedi, A., Activation Energy Impact in Nonlinear Radiative Stagnation Point Flow of Cross Nanofluid, *Int. Commun. Heat Mass Transf.*, vol. **91**, pp. 216–224, 2018.

Khan, M., Rasheed, A., Salahuddin, T., and Ali, S., Chemically Reactive Flow of Hyperbolic Tangent Fluid Flow Having Thermal Radiation and Double Stratification Embedded in Porous Medium, *Ain Shams Eng. J.*, vol. **12**, no. 3, pp. 3209–3216, 2021.

Massoudi, M., Local Non-Similarity Solutions for the Flow of Non-Newtonian Fluid over a Wedge, *Int. J. Non-Linear Mech.*, vol. **36**, pp. 961–976, 2021.

Mushtaq, A., Mustafa, M., Hayat, T., Rahi, M., and Alsaedi, A., Exponentially Stretching Sheet in a Powell-Eyring Fluid: Numerical and Series Solutions, *Z. Naturforsch.*, vol. **68**, pp. 791–798, 2013.

Nazeer, M., Khan, M.I., Rafiq, M.U., and Khan, N.B., Numerical and Scale Analysis of Eyring-Powell Nanofluid towards a Magnetized Stretched Riga Surface with Entropy Generation and Internal Resistance, *Int. Commun. Heat Mass Transf.*, vol. **119**, pp. 0735–1933, 2020.

Powell, R.E. and Eyring, H., Mechanism for Relaxation Theory of Viscosity, *Nature*, vol. **154**, pp. 427–428, 1944.

Rahimi, J., Ganji, D.D., Khaki, M., and Hosseinzadeh, Kh., Solution of the Boundary Layer Flow of an Eyring-Powell Non-Newtonian Fluid over a Linear Stretching Sheet by Collocation Method, *Alexandria Eng. J.*, no. **56**, pp. 621–627, 2017.

Rasool, G. and Zhang, T., Characteristics of Chemical Reaction and Convective Boundary Conditions in Powell-Eyring Nanofluid Flow along a Radiative Riga Plate, *Heliyon*, vol. **5**, p. e01479, 2019.

Ray, A.K., Vasu, B., and Murthy, P.V.S.N., Non-Similar Solution of Eyring–Powell Fluid Flow and Heat Transfer with Convective Boundary Condition, Homotopy Analysis Method, *Int. J. Appl. Comput. Math.*, vol. **6**, p. 16, 2020.

Razzaq, R. and Farooq, U., Non-Similar Forced Convection Analysis of Oldroyd-B Fluid Flow over Exponentially Stretching Surface, *Adv. Mech. Eng.*, vol. **13**, no. 7, 2021.

Sajid, T., Sagheer, M., Hussain, S., and Bilal, M., Darcy-Forchheimer Flow of Maxwell Nanofluid Flow with Nonlinear Thermal Radiation and Activation Energy, *Am. Inst. Phys. Adv.*, vol. **8**, p. 035102, 2018.

Shawgo, R.S., Grayson, A.C.R., Li, Y., and Cima, M.J., BioMEMS for Drug Delivery, *Curr. Opin. Solid State Mater. Sci.*, vol. **4**, pp. 329–334, 2002.

Sheikholeslami, M., Bandpy, G., Ellahi, R., Hassan, M., and Soleimani, S., Effects of MHD on Cu-Water Nanofluid Flow and Heat Transfer by Means of CVFEM, *J. Magn. Magn. Mater.*, vol. **349**, no. 1, pp. 188–200, 2014.

Sparrow, E.M. and Yu, H.S., Local Non-Similarity Thermal Boundary Layer Solutions, *ASME J. Heat Transf.*, vol. **93**, pp. 328–334, 1971.

Sparrow, E.M., Quack, H., and Boerner, C.J., Local Non-Similarity Boundary-Layer Solutions, *AIAA J.*, vol. **8**, no. 11, pp. 1936–1942, 1970.

Tiwari, K.R. and Das, M.K., Heat Transfer Augmentation in a Two-Sided Lid-Driven Differentially Heated Square Cavity Utilizing Nanofluids, *Int. J. Heat Mass Transf.*, vol. **50**, pp. 2002–2018, 2007.

Turkyilmazoglu, M., Exact Analytical Solutions for Heat and Mass Transfer of MHD Slip Flow in Nanofluids, *Chem. Eng. Sci.*, vol. **84**, no. 2, pp. 182–187, 2002.

Tyler, T., Shenderova, O., Cunningham, G., Walsh, J., Drobnik, J., and McGuire, G., Thermal Transport Properties of Diamond Based Nanofluid and Nanocomposites, *Diamond Related Mater.*, vol. **15**, pp. 2078–2081, 2016.

Waqas, M., Jabeen, S., Hayat, T., Shehzad, S., and Alsaedi, A., Numerical Simulation for Nonlinear Radiated Eyring-Powell Nanofluid Considering Magnetic Dipole and Activation Energy, *Int. Commun. Heat Mass Transf.*, vol. **112**, no. 1, p. 104401,

2020.

Yu, W., France, D.M., Routbort, J.L., and Choi, S.U.S., Review and Comparison of Nanofluid Thermal Conductivity and Heat Transfer Enhancement, *Heat Transf. Eng.*, vol. **29**, pp. 432–460, 2008.